A PROCESS FOR ICE DETECTOR PLACEMENT USING 3-D EULERIAN DROPLET IMPINGEMENT ANAYSIS

by

GLENN T. LANCASTER

Presented to the Faculty of the Graduate School of

The University of Texas at Arlington in Partial Fulfillment

of the Requirements

for the Degree of

MASTER OF SCIENCE IN AEROSPACE ENGINEERING

THE UNIVERSITY OF TEXAS AT ARLINGTON

December 2008

ACKNOWLEDGEMENTS

The author recognizes and appreciates the efforts of Fran Booth and Roger Aubert, who provided the opportunity to work on the subject matter of this paper. Thanks to Jason Wright for sharing his knowledge of aircraft ice accretion and for his efforts in ice tunnel testing.

December 26, 2008

ABSTRACT

A PROCESS FOR ICE DETECTOR PLACEMENT USING 3-D EULERIAN DROPLET IMPINGEMENT ANAYSIS

Glenn T. Lancaster, M.S.

The University of Texas at Arlington, 2008

Supervising Professor: Donald R. Wilson

Ice detectors invoke an aircraft's ice protection systems, which reduce the risks of flight into known icing conditions. A process has been developed to place ice detectors on aircraft using high fidelity computational icing tools. Three-dimensional Eulerian droplet impingement analysis is used to determine the necessary ice detector height and location required to achieve full functionality. This method is applied to the V-22 Osprey tiltrotor aircraft for validation against both tunnel and flight test data. When compared to icing tunnel test data, computational results for the volume of ice accreted on an antenna were within ten percent, validating the computational tools. Flight test data also provided validation of the ice detector placement method, when both flight test and computational results confirmed that one particular ice detector was ineffective during a flight in known icing conditions.

TABLE OF CONTENTS

LIST OF ILLUSTRATIONS

CHAPTER 1

INTRODUCTION

Ice detectors invoke an aircraft's ice protection systems, which reduce the risks associated with flight into known icing conditions. These risks include both reduction in aerodynamic performance and damage from shedding ice. Ice accretion increases aircraft drag and weight, while reducing lift. Shedding ice can impact the aircraft downstream, damaging control surfaces. It can also be ingested by the engine, damaging stators and other critical components. Tiltrotor aircraft are more susceptible to foreign object damage (FOD) due to shedding ice than most fixed-wing or traditional rotorcraft. The rotors are located in close proximity to the fuselage and in the path of ice shedding from the nose. It is therefore crucial to detect icing conditions early, in order to prevent or minimize ice accretions.

The V-22 tiltrotor aircraft has been the subject of recent Bell-Boeing icing tests in an effort to obtain icing qualification. Icing qualification is primarily supported by in-flight and ice tunnel test data (hereinafter referred to simply as "test data"). However, these tests can be costly, and test conditions are limited. Optimal conditions for icing flight tests are limited to winter months in select locations, while icing tunnel tests are limited by the available tunnel conditions. These tunnel conditions must be scaled to correlate with flight test conditions. Test sections are also limited in size and are therefore only appropriate for testing scale models, or individual components (wing sections, antennae, etc.), rather than an entire full scale aircraft.

Test data can be supplemented by computational fluid dynamic (CFD) analysis, reducing the amount of testing required, and providing additional insight for dynamic configurations or conditions not achieved during testing. CFD also provides the ability to conduct full-scale icing analysis at any time of the year, regardless of outside weather conditions. Computational icing work has traditionally relied heavily on two-dimensional methods, such as LEWICE 2-D [1], which provides analysis of wing sections or engine inlet

profiles. More recently three-dimensional tools have become a viable option with increases in computational resources (for example, the use of multi-computer architecture for parallel compilations). LEWICE 3-D [2], which applies LEWICE 2D methods of ice accretion along the streamlines of a 3-D surface, is being used to generate 2-D ice accretions on 3-D surfaces. Alternatively, FENSAP-ICE [3] employs a fully three dimensional approach to in-flight icing.

I have developed a process to place ice detectors on aircraft using the high fidelity computational icing tools of FENSAP-ICE. Three-dimensional Eulerian droplet impingement analysis is used to determine the necessary ice detector height and location required to achieve full functionality. This process is applied to the V-22, laying a foundation for increased use of CFD during icing qualification at Bell Helicopter.

A summary of aircraft icing is presented followed by validation of the FENSAP-ICE computational tools. To conclude, the process for ice detector placement is developed and results are presented for the V-22.

CHAPTER 2

ICING BACKGROUND

2.1 Aircraft Icing Hazards

When atmospheric conditions are suitable, ice accretion is possible on numerous aircraft surfaces, creating serious safety concerns. Leading edge icing of wing surfaces is the most common and widely studied occurrence of aircraft icing. As streamlines converge on the leading edge, a stagnation point develops, creating an ideal location for droplets to collect. In fact, stagnation points are points of maximum droplet collection efficiency, the ratio of water collected to the maximum water catch [4]. The collected moisture changes to ice in low temperatures.

To illustrate the detrimental effects of ice accretion it is convenient to observe the penalties of airfoil icing. Small ice accretions which conform to the leading edge as an extension of the airfoil have the least impact, although performance is still reduced. According to [4], these smaller accretions can reduce the maximum lift coefficient, Cl_{max}, up to 30% and increase drag by as much as 100%. Larger accretions with horn shapes, discussed in the following ICE TYPES section, can reduce Cl_{max} by 40% and increase drag by 200% (Fig. 2.1). These percentages are heavily dependent on the size and shape of the ice, as well as its surface roughness.

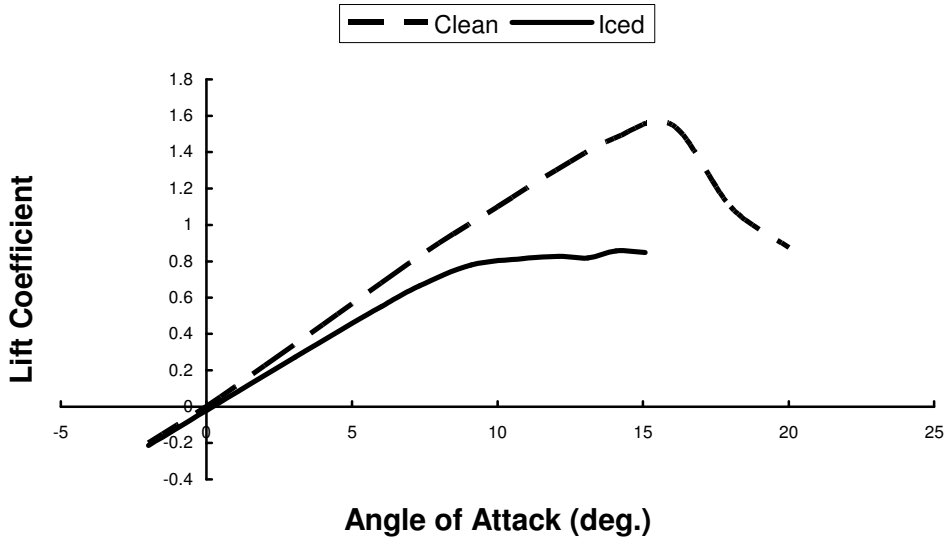

(a)

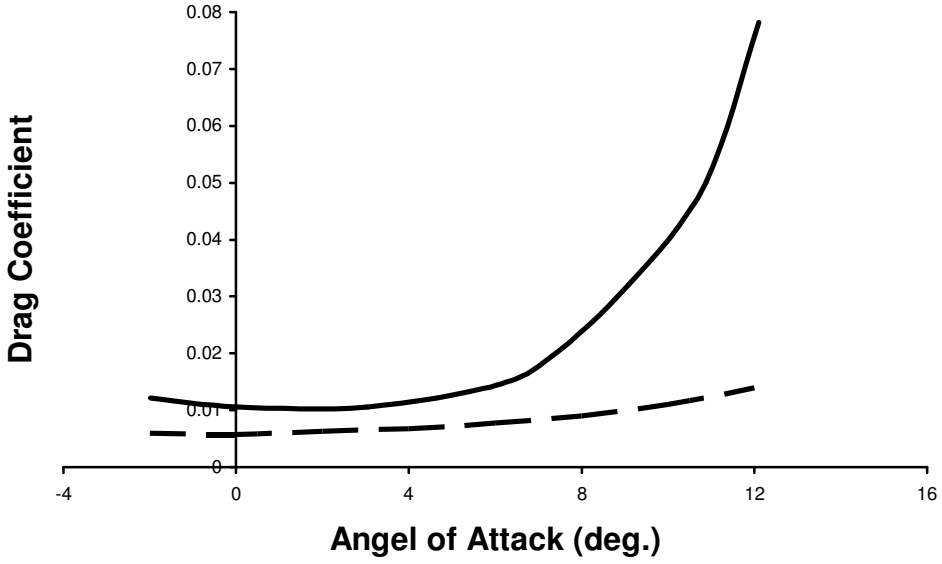

(b)

Fig. 2.1 Comparison of (a) lift coefficient, and (b) drag coefficient
for clean [5] and iced [6] NACA 0012 airfoils

Extending the prior discussion of airfoil icing to aircraft wings introduces flight safety concerns. Decreased performance due to leading edge icing results in decreased airspeed and

increased power required, but it can also increase stall speed by one half of the percent decrease in Cl_{max}. For example, if Cl_{max} is decreased by 30% then stall speed will increase by 15% [4]. Aileron effectiveness may also be compromised as the wing icing alters flow over control surfaces.

It is common for many other surfaces on the aircraft to accrete ice, creating additional hazards. Some prime examples are the empennage control surfaces. Typical empennage surfaces are in fact more efficient collectors than wings since their airfoil sections are thin. Thus they collect droplets and accumulate ice at a faster rate than wings. In the worst cases, loss of control of the aircraft can occur.

Other potential locations for accretion include exposed instrumentation and antennae which are often positioned near the aircraft's nose in areas prone to icing. In fact any surface may become an ice collector if suitably located. Windshields, engine inlets and rotor blades are among other ice accumulators. These ice accretions, in particular those near the aircraft's nose, create a potential for FOD. FOD due to ice shedding is a serious concern which can manifest in three ways. As accumulations grow, aerodynamic forces can cause ice to break free from the aircraft's surface. Vibratory loads may also shake masses of ice loose. Finally, as the aircraft leaves icing conditions, increased temperature causes the ice to melt slightly, reducing its adhesion to the aircraft. As a mass of ice sheds from the aircrafts surface it turns into a projectile and the potential for FOD is realized. Ice accumulates and breaks free in irregular shapes. Aerodynamic forces on the irregularly shaped mass make its trajectory difficult to accurately predict. This is especially true since every accumulation and shed is different. FOD has been observed to take chunks out of rotors and break holes in control surfaces. Ice can also be ingested into engines, damaging stators and even causing engine failures.

The cause of these ice accretions is the presence of moisture in the form of super cooled liquid droplets, and the acquiescence of local flow conditions. While it may be intuitive that extreme cold would bring the onset of ice accretion, a less obvious trigger for aircraft icing

is moderately cold atmospheric temperature near freezing. In this moderately cold weather, temperatures across the aircraft can vary far below freestream conditions. With the addition of moisture in the form of clouds, potentially hazardous ice accretion becomes a reality.

2.2 Ice Types

There are two primary types of ice accretions, rime and glaze ice. The shape and extent of these ice formations are dependent on the Liquid Water Content (LWC) of the cloud, droplet diameter, air temperature, flight speed, angle of attack, altitude, aircraft geometry, and the duration of the icing encounter.

Rime ice is characterized by an opaque white appearance, the result of air being introduced into the accretion. This type of ice is less dense and more fragile as a result. Under rime ice conditions, moisture simply hits and sticks, freezing almost instantly to the aircraft's surface. Certain conditions lend themselves to rime ice accretion, including low atmospheric temperature (below 20 F˚), relatively low LWC, lower airspeeds, and small droplet diameters. Figure 2.2 shows an illustration of typical rime ice accretion. Since the droplets freeze quickly, the ice shape grows in the direction of the impinging flow and conforms to the leading edge of the airfoil.

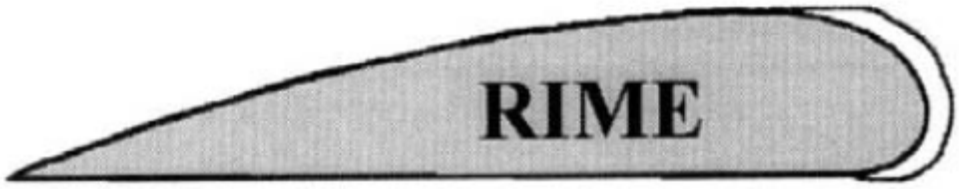

Fig. 2.2 Airfoil section with rime ice accretion [4]

In moderately cold conditions, above 20 F˚, water droplets may strike an aircraft surface and run back before freezing, creating glaze ice. Glaze ice has a glossy or wet appearance and is transparent. The term clear ice has been used to describe glaze ice, which conforms to airfoil sections or surfaces of the aircraft, although the two terms are often used

interchangeably. Alternatively, large glaze ice accretions may form either a lobster tail or horns (Fig. 2.3) on the leading edge of airfoils, a result of water run back. In any case, glaze ice is slower freezing than rime ice, creating a denser, harder accretion. Conditions that contribute to glaze icing consist of temperatures close to the freezing point (20 to 32 F˚), high LWC, high airspeed, and large droplet diameters.

Fig. 2.3 Airfoil section with glaze ice accretion with horns [4]

Rime and glaze describe the two categories of ice which accrete on aircraft, although a third category should be defined in which both ice types are present. Mixed, or intermediate ice, is the presence of rime and glaze ice in combination. As one would assume, the temperature range for such an accretion overlaps both the rime and glaze ranges. Mixed accretions tend to occur between 10 and 25 F˚, with glaze ice near stagnation and rime ice farther aft.

2.3 Testing

Testing has long been used to predict ice accretion on aircraft, and while it is a useful and necessary tool for certification, it does not always solve the entire problem or answer all questions regarding ice accretion. Icing tunnels are typically used to simulate accretion on individual components or scale models of aircraft, due to limitations on the size of the test section. Some of the largest test sections include the NASA Glenn Icing Research Tunnel (6' by 9') and the Boeing Research Aero-Icing Tunnel (4' by 6'). Antenna, wing sections,

empennages, and engine cowling have all been tested in icing tunnels, but testing of components does not always represent the installed flight conditions. Ice tunnels are limited by the conditions they are capable of reproducing, and test conditions must be scaled to approximate true flight conditions. In addition, testing is generally not recommended below 1/2 model scale. In spite of their drawbacks ice tunnels continue to be a valuable tool in icing certification.

Full scale tests of aircraft are few and far between. There are simply logistical problems associated with testing a full scale aircraft, although icing tankers have been used in some instances to spray droplets from the leading aircraft onto trailing aircraft. For large planes or tiltrotors, the icing tanker may only be capable of spraying one portion of the aircraft at a time.

Flight test is the last stage of icing certification, but success is a challenge that requires a significant effort. Meteorologists are employed to predict weather conditions capable of producing ice on the aircraft, and testing is inherently limited by the atmosphere, time of year, and location. This requires that the aircraft be tested during winter months in northern regions where suitable icing conditions are frequent. Testing is instrumental in reducing the risks associated with aircraft icing.

2.4 Alleviation

Unintentional flight into icing conditions may represent the highest risk of any icing related peril. For aircraft without ice protection systems, the only corrective action is to exit the icing cloud before accumulations cause severe problems. Today, more aircraft are designed with the intent to fly into known icing conditions in order to meet customer's needs. These aircraft must be certified for such flight through the aforementioned testing. Certification also requires the ability to prevent or remove ice accretions with ice protection systems.

In order to prevent or alleviate ice accretion, several techniques are employed which fall into the categories of de-icing, which is reactive, or anti-icing, which is preventative. One de-icing technology is the pneumatic boot, which is frequently positioned on the leading edge of wing sections, and when inflated, breaks free any accumulated ice. Hot air methods, which are

used for anti-icing, work by blowing hot air onto the interior surface of the aircraft's skin, evaporating moisture from the exterior surface. Electro-thermal heating is typically employed on surfaces not suitable for other techniques. Electro-thermal heating applied continuously has an anti-icing effect, while application in cycles is used for de-icing. Particular electro-thermal applications include windshields and rotor blades.

2.5 Detection

In order to protect an aircraft from ice accretion, it is necessary to determine when the aircraft is flying in icing conditions. Ice detectors automatically determine if the aircraft is in such conditions in order to trigger ice protection systems. Ice detectors work by accreting small amounts of ice and must be placed on the aircraft such that they will experience freestream icing conditions. One common type is the vibrating probe ice detector. The vibration frequency of the probe decreases as ice accumulates on its surface. Traditionally, empirical knowledge and handbook methods are used to place detectors on aircraft. However, it can be difficult to predict the effectiveness of ice detectors using these methods.

On the aircraft, shadow zones correspond to areas where ice detectors do not effectively register ice. Handbook methods can be used to estimate the thickness of a shadow zone based on simple shapes and lengths [7]. In reality, aircraft with complex geometries have shadow zones that are highly three dimensional, thus simple methods for computing shadow heights are not completely accurate. In order to ensure that ice detectors will function properly, icing flight tests are conducted over a wide range of conditions. If the detectors are not placed effectively, they must be moved and retested, assuming atmospheric conditions cooperate. CFD can be applied prior to flight test to determine the effectiveness of ice detectors as well as to predict ice accretions on the aircraft.

CHAPTER 3

CFD ICING BACKGROUND

The use of CFD to predict aircraft icing can reduce icing certification time and cost. Icing tests, whether in-flight or in an icing tunnel, are expensive and time consuming endeavors. The tests themselves involve numerous individuals from pilots to meteorologists to engineers specializing in icing certification. Preparation and modification of the flight test vehicle or ice tunnel models require an extensive amount of time and the cost is significant. CFD can provide relief, as a single engineer can simulate aircraft icing using high performance computing resources at a moderate cost.

3.1 2-D Methods

Early development of CFD icing methods has been focused on 2-D analysis. NASA LEWICE [1] has been a staple of 2-D computational icing work since the early 90's. Initially, potential flow methods were used to predict flow around airfoil sections, or through engine inlet profiles. LEWICE, for example, employed a Douglas Hess-Smith panel code to compute potential flow solutions. With increased computational resources resulting in reduced turnaround time, Euler and Navier-Stokes methods became viable incorporating compressibility and viscosity effects. Regardless of the fidelity of the 2-D flow solution, the LEWICE approach for computation of droplet impingement is to determine the droplet trajectory by solving ordinary differential equations for arbitrarily-shaped particles. This simulation involves releasing droplets upstream and, using a previously computed flow solution, calculating the path of the droplets around an object, or until the point of impingement. Thermodynamic computation, used to determine ice accretion, is based on a modified Messinger model [8] using the collection efficiency as input and outputting an ice growth rate on the surface of the subject.

3.2 Quasi-3-D Methods

The development of quasi 3-D icing codes created the ability to analyze complete aircraft in icing conditions. LEWICE3D [2] is one such code which uses 3-D Hess-Smith panel code for computing the flow solution, and once again ordinary differential equations to represent the droplet trajectories. In the same manner as 2-D LEWICE, droplet paths are determined by releasing droplets upstream of the subject and tracking them downstream toward impingement, or until the droplets pass the area of interest. Of course, the droplet paths being computed are three dimensional in nature. The thermodynamic model used for ice accretion is drawn from the two-dimensional NASA LEWICE code. In the quasi-3-D code, 2-D ice accretions are calculated along surface streamlines. LEWICE3D has also been modified to accept 3-D Navier-Stokes input from third party flow solvers in order to increase accuracy on complex geometry. By applying ordinary differential equations and computing 2-D heat transfer along surface streamline of 3-D geometries, LEWICE3D has successfully predicted 2-D ice shaped, at sections of interest, with impressive speed.

3.3 Fully 3-D Methods

With high performance computing resources readily available, a push is being made for high fidelity computational tools in all areas of analysis. In the realm of computational icing, FENSAP-ICE [3], a suite of codes developed by Newmerical Technologies International, fills that role. It is a fully three-dimensional in-flight icing analysis tool, capable of computing a water droplet field solution via an Eulerian description of two-fluid flow and 3-D ice shapes using partial differential equations on the aircraft's surface. This is in contrast to the Lagrangian particle tracking and heat transfer computations along streamlines, typically applied in 2-D and quasi-3-D methods. Predicting effectiveness of ice detectors on three dimensional aircraft requires high fidelity air solutions, and droplet impingement, thus FENSAP-ICE was selected for this research, and its methods are discussed in more detail throughout the following chapters.

CHAPTER 4

CFD ICING PROCESS

In a broad sense, the FENSAP-ICE process of icing analysis is the same as the original LEWICE 2-D approach. The process consists of computing a flow solution, followed by droplet impingement analysis yielding collection efficiency, and finally ice accretion calculation as a function of time. The fidelity of each step of the process, however, has increased significantly.

4.1 Aerodynamic Flow Solution

The FENSAP flow solver is a finite element solution of 3D turbulent Reynolds-averaged Navier-Stokes equations. The finite element method employed is inherently robust, allowing difficult geometries to be analyzed, and the use of unstructured grids allows complex details of aircraft to be captured with minimal effort. For instance, antenna and instrumentation can be captured in order to predict ice accretions which affect performance of these systems. Boundary layer resolution is accomplished using prism elements grown from the surface in order to satisfy turbulence modeling requirements. In this research, the Spalart-Allmaras one equation turbulence model is applied, along with the following equations for continuity, momentum, and energy.

$$\vec{\nabla} \cdot \left(\rho_a \vec{u}_a \right) = 0 \tag{4.1.1}$$

$$\vec{u}_a \cdot \vec{\nabla} \left(\rho_a \vec{u}_a \right) = \vec{\nabla} \sigma^{ij} \tag{4.1.2}$$

$$\vec{\nabla} \cdot \left(\rho_a \vec{u}_a H \right) = \vec{\nabla} \left(\kappa \left(\vec{\nabla} T \right)^j + v_i \tau^{ij} \right) \tag{4.1.3}$$

Density, ρ_a, and velocity, u_a, are local values for air. The stress tensor, temperature, shear stress, enthalpy, viscosity, and thermal conductivity are represented as σ, T, τ, H, υ, κ respectively. Solution of the full partial differential equations, including the energy equation (as opposed to adiabatic or isotropic assumptions), is necessary to compute the heat transfer coefficient required for ice accretion computations.

4.2 Eulerian Droplet Impingement

Droplet impingement analysis is the computation of Liquid Water Content (LWC) and droplet velocities. The N-S flow solution is used as input into the droplet impingement computation. It is assumed that the droplets do not affect the air solution since the liquid water content concentration is very low (on the order of 0.5 g/m^3), thus the droplet and air equations are decoupled. The DROP3D module of FENSAP-ICE is an Eulerian two-fluid model using the Navier-Stokes dry air equations, and the following continuity and momentum equations applied to water concentration [9].

$$\frac{\partial \alpha}{\partial t} + \vec{\nabla} \cdot \left(\alpha \vec{\mathbf{u}}_d \right) = 0 \tag{4.2.1}$$

$$\frac{\partial \vec{\mathbf{u}}_d}{\partial t} + \vec{\mathbf{u}}_d \cdot \vec{\nabla} \vec{\mathbf{u}}_d = \frac{C_D \, \mathrm{Re}_d}{24K} \left(\vec{\mathbf{u}}_\mathbf{a} - \vec{\mathbf{u}}_d \right) + \left(1 - \frac{\rho_\mathbf{a}}{\rho_w} \right) \frac{1}{Fr^2} \vec{g} \tag{4.2.2}$$

In these equations, α is the water volume fraction, and u_d is the droplet velocity. The terms u_a, ρ_a, ρ_w, C_D Re_d, Fr, K, represent the air velocity, air and water densities, droplet drag coefficient, droplet Reynolds number, Froude number, and inertial parameter respectively. The first term on the right hand side of the momentum equation represents the drag on the droplet. The second term includes the effects of buoyancy and gravity. The drag coefficient is represented by the following empirical equations based on spherical droplets [10].

$$C_D = \left(24 / \mathrm{Re}_d \right) \left(1 + 0.15 \mathrm{Re}_d^{\,0.687} \right) \text{ for } \mathrm{Re}_d \le 1300 \tag{4.2.3}$$

$$C_D = 0.4 \text{ for } \mathrm{Re}_d > 1300 \tag{4.2.4}$$

The water concentration, or droplet, equations are solved via finite element method at each node of the computational domain where air velocities are known, eliminating the need for Lagrangian particle tracking.

Boundary conditions are applied to the farfield as a freestream droplet velocity and water concentration, analogous to freestream velocity and density boundary conditions for air flow. Surface boundary conditions are not as intuitive, and require some explanation. When a

droplet impacts the surface, it becomes a thin water film. In this way, the water ceases to be a droplet and exits the computational domain. Inversely, water does not enter the computational domain from the surface. Thus, the appropriate boundary condition to apply is

$$-\alpha\vec{\mathbf{u}}_d \cdot \vec{\mathbf{n}} \geq 0 \tag{4.2.5}$$

which can be implemented by clipping or nullify the droplet velocity normal $u_d \cdot n$ to the wall.

The results DROP3D are a field solution of droplet velocities and a collection efficiency distribution on the 3D surface. In the presented application, collection efficiency is defined as

$$\beta = \vec{\mathbf{u}}_d \cdot \vec{\mathbf{n}} \tag{4.2.6}$$

Validation of the DROP3D module can be found for impingement limits on a 2-D cylinder and a 3-D sphere in [11].

4.3 Ice Accretion

Ice accretion is computed following the droplet solution. ICE3D is the corresponding module of FENSAP which computes 3-D ice accretions, using the viscous forces and heat fluxes obtained from the flow solution and collection efficiencies from droplet impingement analysis. The icing module [3] is based on the Messinger model; however partial differential equations are used for three dimensional analyses. Computations are made for conservation of mass and energy along the surface as depicted in the Fig. 4.1.

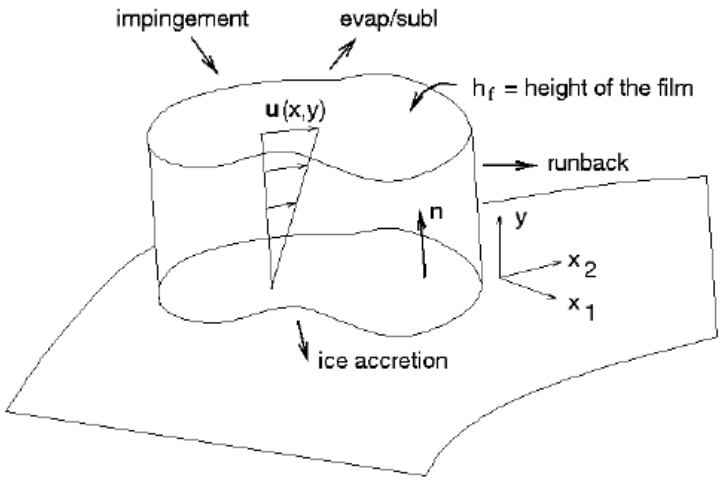

Fig. 4.1 Heat and mass balance in a thin film [12]

The water film accumulated by DROP3D is thin, less than 40 microns for aircraft icing, allowing for a simplified representation of the velocity in the film, u_f. A linear velocity profile normal to the surface is assumed within the film

$$\vec{u}_f(\vec{x}, y) = \frac{y}{\mu_w}\vec{\tau}_{wall}(\vec{x}, y) \tag{4.3.1}$$

and averaged for simplicity.

$$\bar{u}_f(\vec{x}, y) = \frac{1}{h_f}\int_0^{h_f} u_f(\vec{x}, y)dy = \frac{h_f}{2\mu_w}\vec{\tau}_{wall}(\vec{x}) \tag{4.3.2}$$

The film velocity is a function of position $x = (x_1,x_2)$ along the surface, and the distance y measured from the surface to the film height, h_f. After averaging, the velocity becomes a function of film height and shear stress τ_{wall}. Using this approximation for u_f, conservation of mass for the water film can be written as

$$\rho_w\left(\frac{\partial h_f}{\partial t} + \vec{\nabla}\left(\bar{u}_f h_f\right)\right) = U_\infty \cdot LWC_\infty \cdot \beta - \dot{m}_{evap} - \dot{m}_{ice} \tag{4.3.3}$$

where the right hand terms represent droplet impingement, water evaporation, and ice accretion respectively. Conservation of energy is applied through the equation

$$\begin{aligned}\rho_w\left(\frac{\partial h_f C_w \tilde{T}_s}{\partial t} + \vec{\nabla}\left(\bar{u}_f h_f C_w \tilde{T}\right)\right) = &\left(C_w \tilde{T}_{d,\infty} + \left\|\vec{u}_d\right\|^2\right)\times U_\infty \cdot LWC_\infty \cdot \beta \\ &- 0.5\left(L_{evap} + L_{subl}\right)\dot{m}_{evap} \\ &+ \left(L_{fusion} - C_{ice}\tilde{T}\right)\dot{m}_{ice} + \varepsilon\sigma\left(T_\infty^4 - T_s^4\right) + \dot{Q}_h\end{aligned} \tag{4.3.4}$$

in which the terms on the right hand side are heat transfer due to droplet impingement, evaporation, ice accretion, radiation, and convection, in that order. The constants ρ_w, C_w, C_{ice}, L_{evap}, L_{subl}, L_{fusion}, and σ are physical characteristics of water while the terms $T_{d,\infty}$, U_∞, LWC_∞, and T_∞ are ambient values defined by the flight condition. Local collection efficiency β and droplet impact velocity u_d are supplied by the DROP3D solution, while heat flux $\dot{Q}_h$ and shear stress

τ_{wall} are obtained from the air solution. The following compatibility relationships are applied to complete the system of equations, allowing values for h_f, $\tilde{T}$, and $\dot{m}_{ice}$ to be computed.

$$h_f \geq 0 \tag{4.3.5}$$

$$\dot{m}_{ice} \geq 0 \tag{4.3.6}$$

$$h_f \tilde{T} \geq 0 \tag{4.3.7}$$

$$\dot{m}_{ice} \tilde{T} \leq 0 \tag{4.3.8}$$

4.4 Validation of Computational Tools

Validation of the FENSAP-ICE codes against test data and the 2-D LEWICE code has been presented for various icing cases, both 2-D and 3-D. Here, a brief overview is given of two cases presented by other authors, as well as one new antenna icing case analyzed as a part of this author's thesis.

Beaugendre, Morency, and Habashi [3] compare a 2-D analysis, using the 3-D FENSAP tools, of a NACA 0012 airfoil section for 7 minutes of ice accretion. Of particular interest is a comparison made between FENSAP, the 2-D LEWICE code, and experimental data obtained from the NASA Glenn Icing Research Tunnel. Figure 4.2 shows that the limits of the ice shape compare well on the upper surface of the airfoil, while on the lower surface, both CFD codes under predict the accretion compared to the experiment. It is represented by the authors that LEWICE predicts more runback than FENSAP, which explains why FENSAP has a thicker ice shape on the upper surface and is closer to experimental results. The same explanation is given for the lower surface where LEWICE is closer to the test data.

Narramore, et al. [13] present a comparison of icing results for a BA609 wing section. The icing tunnel walls were included in the computation, as was the gap between the wall and the wing section. Results indicate that the location and shape of the computed ice accretion compared well with data from the NASA Glenn IRT, as shown in Fig. 4.3.

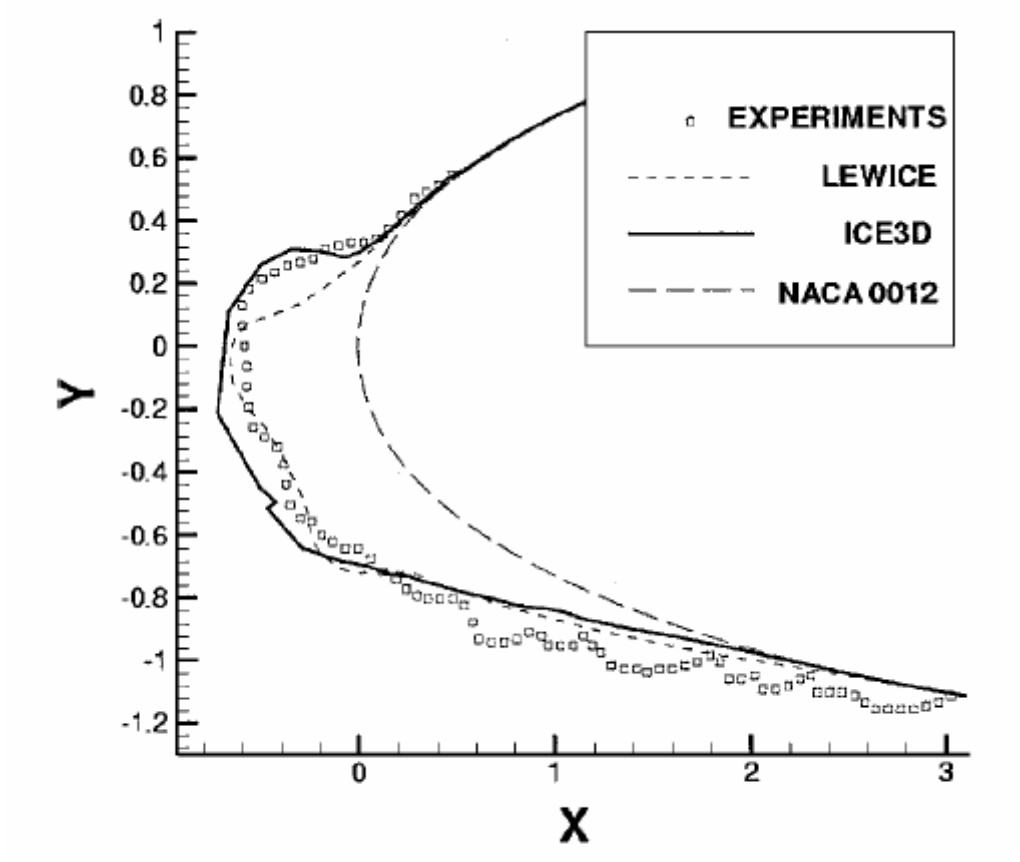

Fig. 4.2 Comparison between ICE3D, LEWICE, and IRT experimental ice shape [3]

(a) (b)

Fig. 4.3 Comparison of (a) computed, and (b) measured ice shapes [13]

As a part of the scope of my work, ice accretion is predicted on an antenna near the nose of the V-22 Osprey tiltrotor, for code validation. Results of this analysis serve as a design aid to reduce ice accretion on the antenna.

A blind study was conducted using FENSAP-ICE in order to quantify the amount of ice being accumulated during flight tests. The CFD model consists of a V-22 fuselage with appendages (Fig 4.4). Flight test conditions were matched with full scale analysis, one of the benefits of computational icing. Figure 4.5 compares the location of the ice accretion after and during flight test (Fig. 4.5 a-b), with the predicted result (Fig. 4.5 c). The accretion is located on the radome's forward face with the bulk of the ice near the tip. The exact amount of ice was not able to be determined from the flight test as melting occurred during descent. The ice shape after landing is smaller with less coverage than that of the computation. Comparison of the computation to the accretion observed during flight test shows a much closer match.

After qualitatively verifying the code's ability to predict ice on the antenna, a design study was undertaken in an effort to reduce the amount of ice being accreted. Three fairings were designed to encapsulate the existing antenna, each having a different sweep angle. The sweep angle was decreased by elongating the radome's forward face, while preserving the overall height, as shown in Fig. 4.6. Following computational analysis, the antenna fairings were tested in the Cox Icing Research Facility icing tunnel [14]. CFD predicted ice accumulations, depicted in the top half of Fig. 4.7, are compared to those of the tunnel test in the lower half of the figure. Sweep angles of 45, 55, and 65 degrees are presented.

Both the CFD and the tunnel test results show accretions covering the forward face of each antenna. Two inverse trends can be observed: 1) as sweep angle increases, ice thickness decreases, 2) the extent of the coverage increases with increasing sweep angle. In effect, the decreased thickness of the ice was counteracted by an increased length, causing the volume of ice accreted on all three fairings to stay within 5% of each other [15]. CFD predicted ice volumes were compared with measurements taken during the icing tunnel test. Predicted volumes proved to be within ten percent of the tunnel test measurements for all three fairings

[15]. With the computational approach validated, CFD was used to compute ice accretions for additional fairing shapes. The final design included a reduction in antenna height, for which CFD predicted a decrease in ice accretion of 30% [15]. Further application of the FENSAP-ICE codes are presented as a part of the following ice detector placement method.

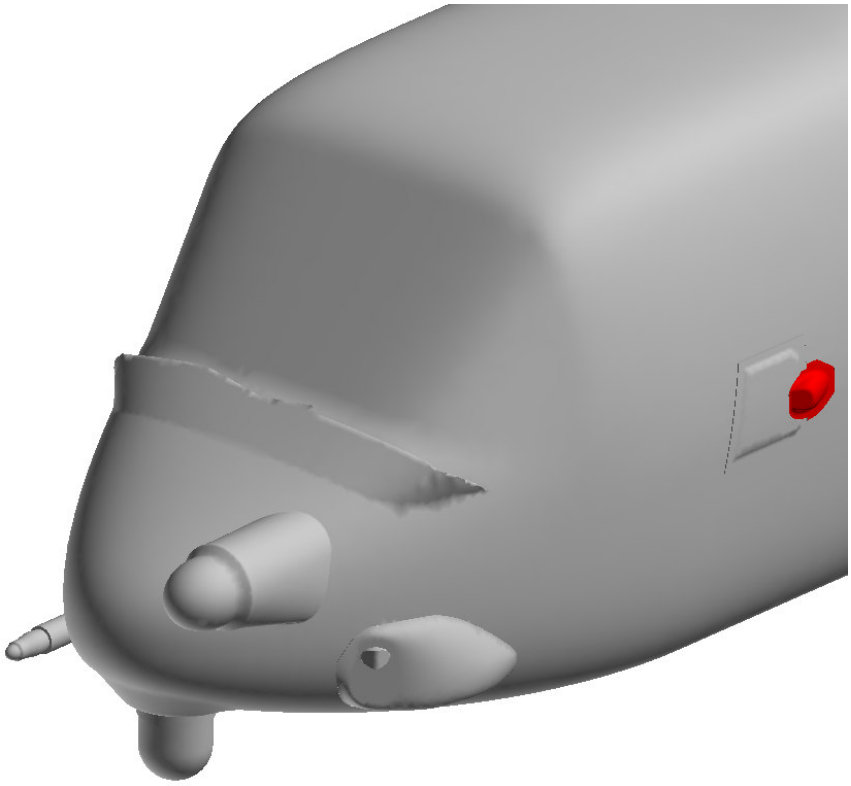

Fig. 4.4 V-22 computational icing model with antenna in red [15]

(a) (b) (c)

Fig. 4.5 Antenna ice accretions (a) experiments after landing,
(b) experiments in-flight, and (c) computation [15]

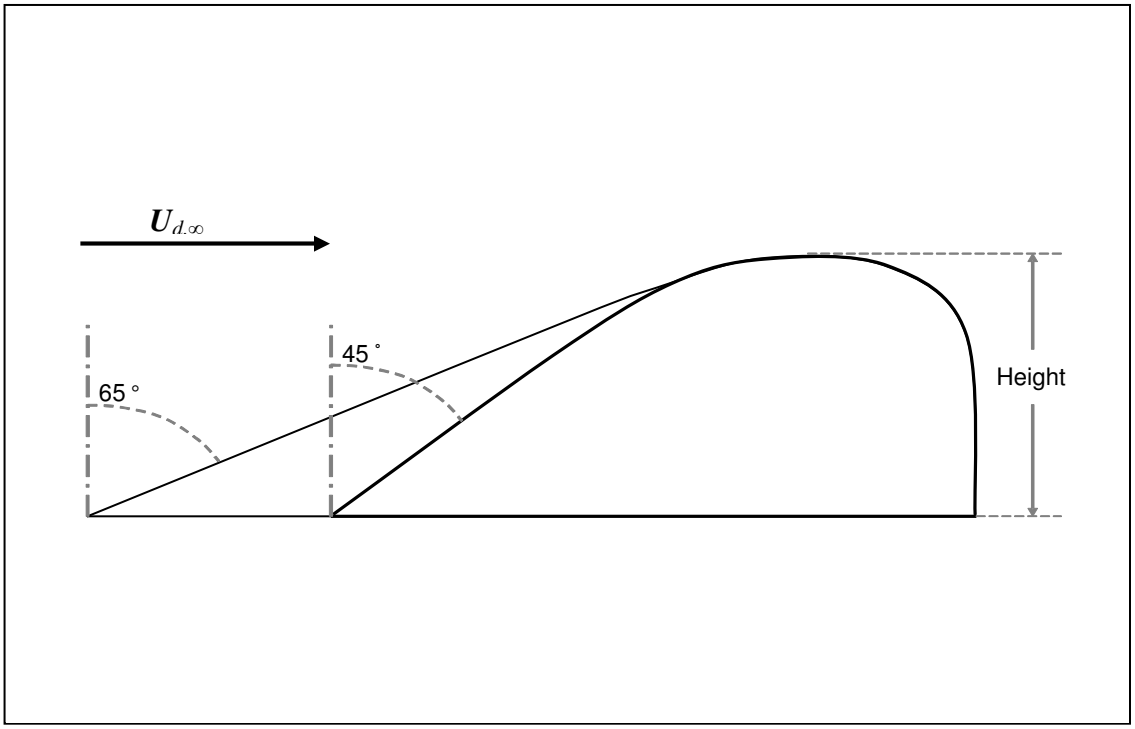

Fig. 4.6 Fairing sweep angle change by extension of forward face

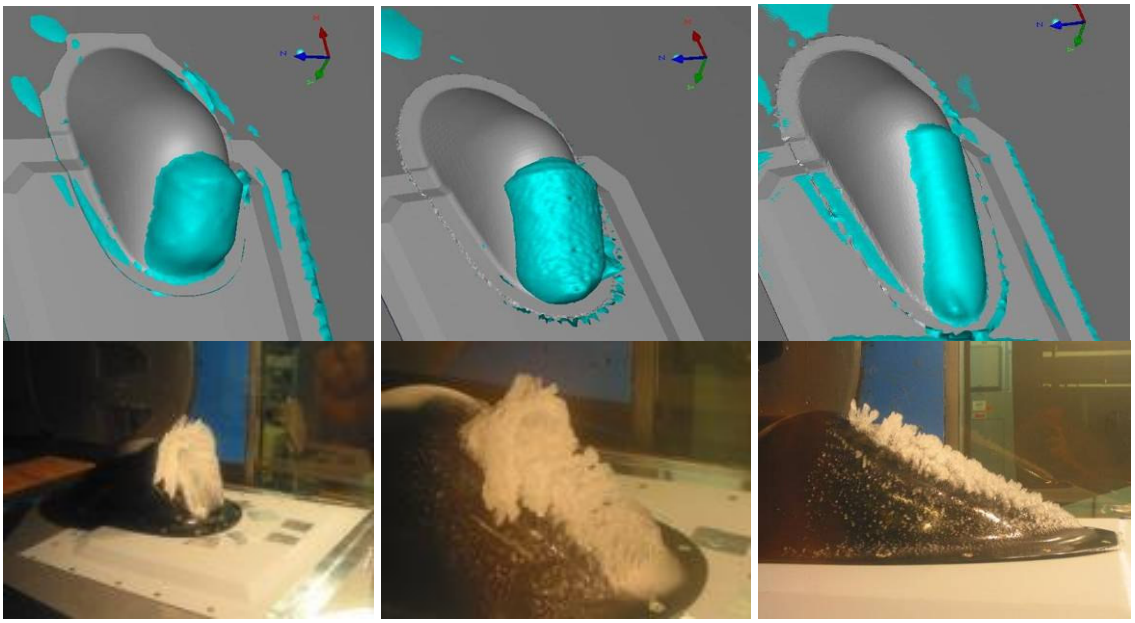

(a) (b) (c)

Fig. 4.7 Ice accretion from CFD (upper), and tunnel test (lower),
for the (a) 45˚, (b) 55˚, and (c) 65˚ antenna fairings [15]

CHAPTER 5

ICE DETECTOR PLACEMENT METHOD

A method for placement of ice detectors has been developed using solutions from the FENSAP-ICE droplet impingement code, DROP3D.

5.1 Shadow Zone Definition

Figure 5.1 shows the DROP3D computed LWC distribution around the V-22 Osprey. The concentration of water is highest away from the aircraft where freestream LWC is present. The results of droplet impingement analysis can be used to define shadow zones. On the aircraft, shadow zones correspond to areas where ice detectors do not effectively register ice.

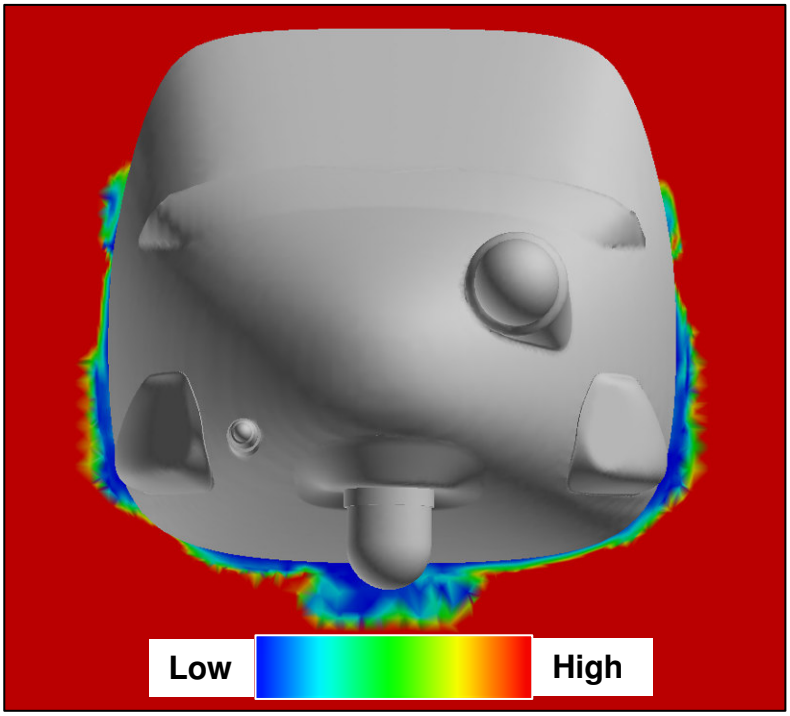

Fig. 5.1 LWC distribution around the V-22 [15]

For Eulerian droplet impingement methods, shadow zones are defined by areas of LWC below a specified threshold. Post-processing the droplet impingement solution using this LWC threshold allows the shadow zone to be viewed as an isosurface in Fig. 5.2.

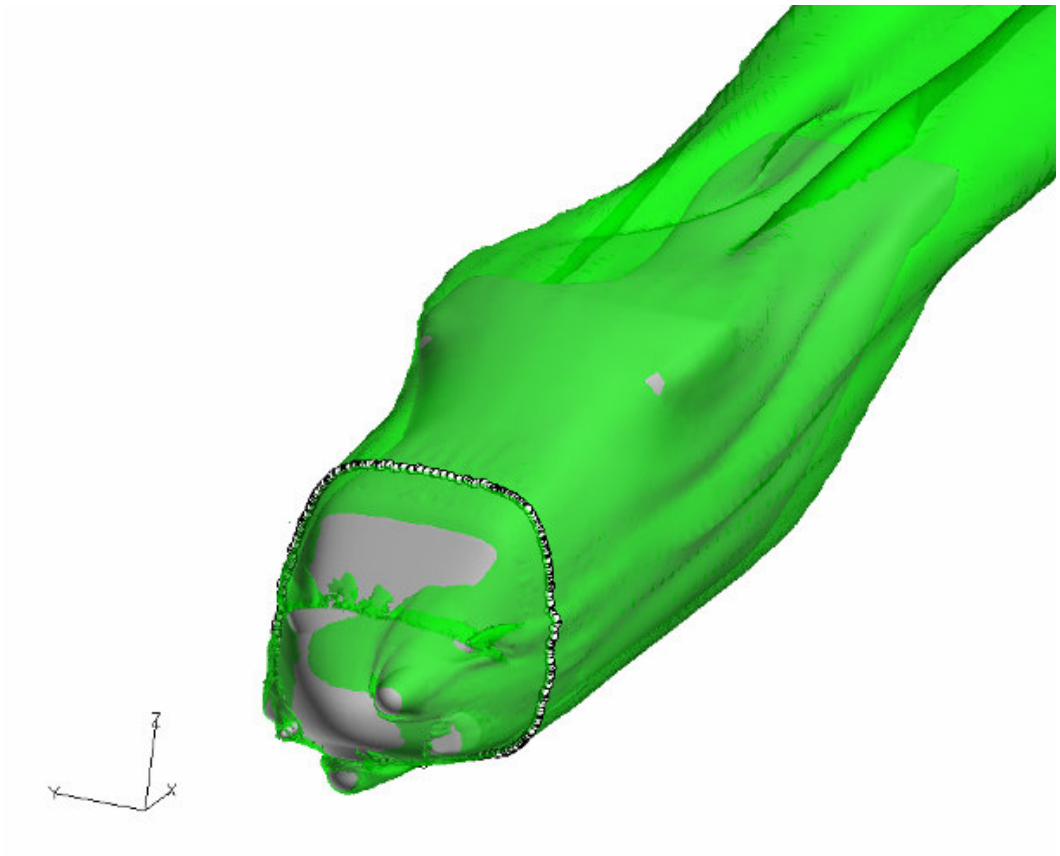

Fig. 5.2 Station of interest indicated on a shadow zone isosurface [15]

An isosurface is a three-dimensional surface representation of points with equal scalar values. The common scalar value in this case is the LWC threshold. The green translucent isosurface wraps around the aircraft defining the limit of the shadow zone. Inside the isosurface, the LWC is lower than the threshold value. LWC is a driving factor for ice accretion, and since ice detectors work by collecting ice, they must extend beyond the shadow and into the freestream where the LWC is high. Therefore, it is appropriate to set a threshold for the shadow zone near freestream LWC, creating the most conservative or largest shadow definition.

As anticipated, there is no shadow on the windshield or nose, indicating that droplets are impinging on the aircraft in these areas. The shadow and fuselage definition are extracted at a specified 2-D station of interest corresponding to an existing or desired ice detector location, as indicated by the previous figure. This method of extracting a shadow definition using isosurface will be referred to as the LWC threshold method.

Alternatively, the droplet impingement solution can be post-processed by a new method in which the result will mimic those of Lagrangian approaches. By creating droplet trajectories based on the Eulerian field solution of droplet velocities, the results become analogous to that of Lagrangian methods, where the shadow zone is defined by the droplet impingement limit (the nearest droplets to the fuselage). Figure 5.3 shows the shadow zones located between the impinging droplets and the aircraft.

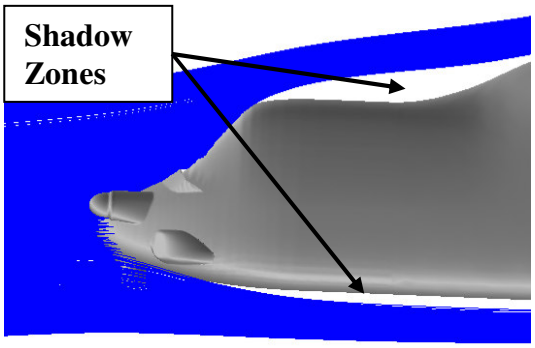

Fig. 5.3 Shadow zones with impinging droplets [15]

Droplet trajectories are created in the same manner as streamlines, though it is important to note that the droplet velocities are used and not the air velocities. Therefore, paths of droplets are computed as opposed to air streamlines. Droplet trajectories are created by seeding a plane upstream of the aircraft with droplet origins and computing droplet paths downstream past the station of interest (Fig. 5.4).

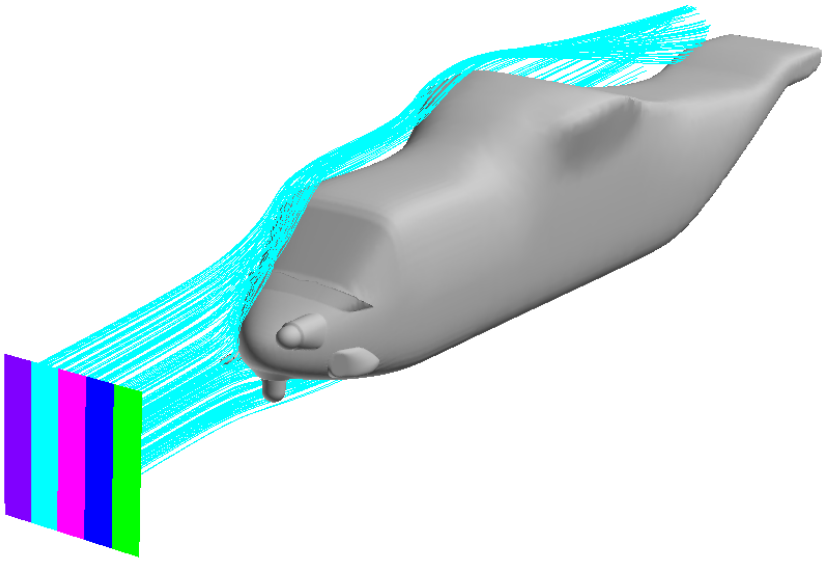

Fig. 5.4 Seed plane with droplet trajectories [15]

The seed plane must be far enough upstream that the droplets are initially free from the influence of the aircraft. If the seed plane is created too close to the aircraft, droplets may originate in inappropriate locations and trajectories will be inaccurate. An appropriate seed plane was selected by examining the droplet perturbation velocities. Figure 5.5 indicates the location of droplet trajectories at a station of interest. The droplets are colored according to

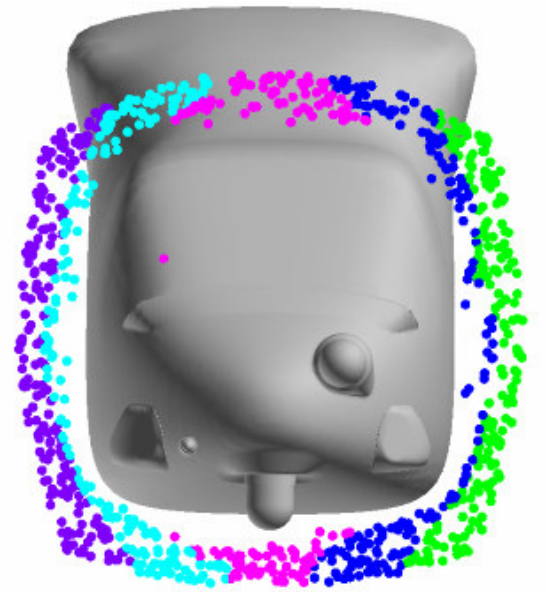

Fig. 5.5 Droplet locations at the station of interest [15]

release locations shown in figure 5.4. The benefit of this method is that it lends itself to a clear definition of the shadow zone by droplet trajectories, without specifying an LWC threshold. This method of extracting the shadow definition by using droplet trajectories will be referred to as the droplet trajectory method.

Correlation was obtained by comparing the shadow generated by this droplet trajectory method with that of the previously discussed LWC threshold method. Both methods render similar results, although either method may result in a slightly larger or smaller shadow at any particular station. When both methods are used concurrently, they provide the most conservative, or largest, shadow zone for ice detector placement.

5.2 Shadow Height Extraction

The droplet shadow, or impingement limit, is extracted from the 3D solution as point data at the station of interest to create Fig. 5.6.

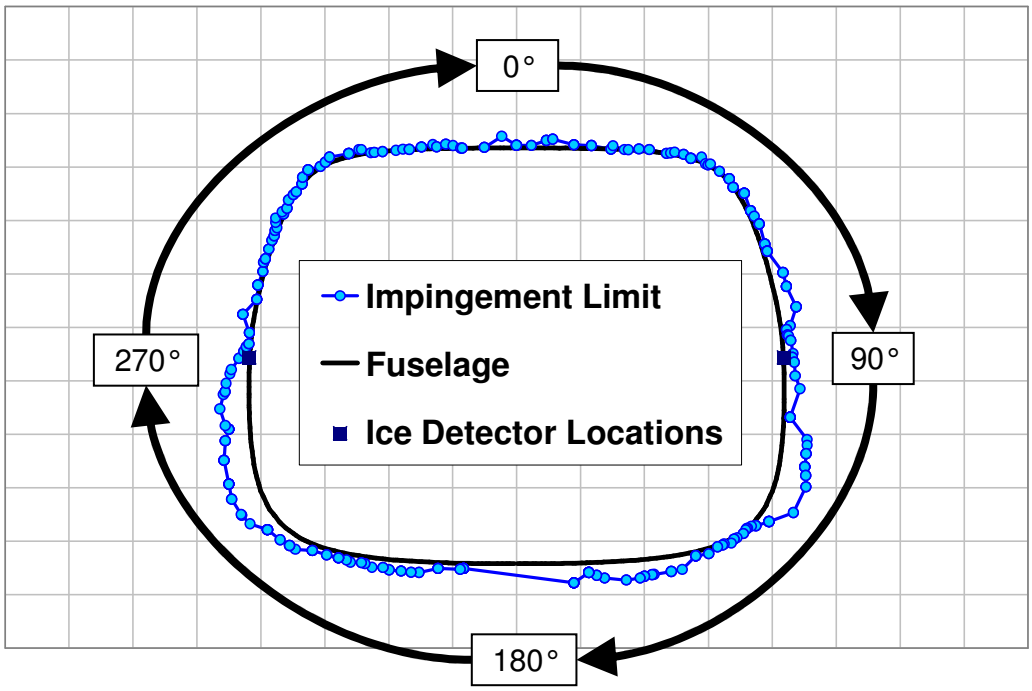

Fig. 5.6 Droplet shadow at the station of interest [15]

The droplet shadow is plotted along with the fuselage geometry, and locations of two ice detectors are indicated at 90˚ and 270˚. Angular position is measured clockwise around the aircraft, looking forward, with zero degrees at the top of the fuselage. The shadow points are centered about the origin and ordered according to angular position by a bubble sort method. After extracting the droplet shadow at the station of interest, the results are transformed to represent the data as shadow height versus angular position, where shadow height is the distance between the aircraft and the shadow, or droplet impingement limit (Fig. 5.7).

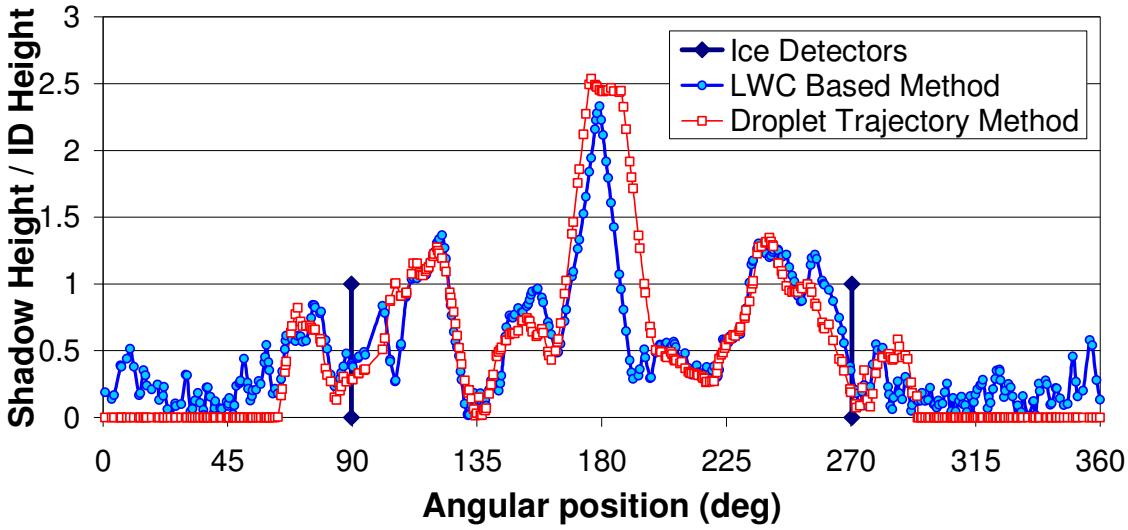

Fig. 5.7 Comparison of results for shadow height methods [15]

The shadow height at a particular angular position on the station of interest is calculated using the nearest shadow point to a given fuselage point. This closest point method was chosen because of its conservative characteristics. In the case for which only a sparse set of shadow points are available, the nearest point method over predicts the shadow height between data points. Methods which interpolate between shadow points can in some cases under predict the shadow height. The process of computing droplet shadows was automated and the results fed directly into a plotting utility. Shadow heights for both the LWC threshold and droplet trajectory methods are plotted together for comparison.

The resulting plot is a quantitative representation of the shadow height at a particular station. For an ice detector to be fully effective, it should exceed the shadow height, putting the detector in freestream icing conditions where the potential for ice accretion is greatest. Figure 5.7 confirms that both the 90˚ and 270˚ ice detectors at this station of interest will function properly. By examining the droplet shadow at 2-D stations, ice detectors can be placed and sized effectively.

This method was validated using V-22 flight test data from a vibrating probe ice detector. In one instance this detector did not register ice during flight in known icing conditions. The particular size of droplet encountered was such that the droplet trajectories moved away from the aircraft's surface, creating a shadow height greater than that of the ice detector and preventing the detector from signaling the ice protection system. Flight conditions, including droplet size and LWC, were recorded by the aircraft's testing instrumentation. The aircraft was then analyzed at these same flight conditions by applying the presented ice detector placement method to determine the effectiveness of the ice detector in question. Results of the computational analysis confirmed that the ice detector was not effective at the recorded conditions.

CHAPTER 6

CONCLUSIONS

As a result of the work performed, a process has been developed to guide the placement of ice detectors on aircraft using CFD. Through application of the developed process, ice detectors can be located and sized appropriately according to the local shadow height.

The process involves an Eulerian droplet impingement solver that provides a field solution of LWC and droplet trajectories. The solver allows a shadow height to be determined anywhere on the aircraft, below which an ice detector will not be fully functional. Two methods of extracting a droplet shadow from the Eulerian solution have been compared for the V-22 tiltrotor:

1) the LWC threshold method uses an isosurface of 100% free-stream LWC to define the shadow, and
2) the droplet trajectory method uses droplet paths created from the droplet field solution trajectories to define the shadow.

Using either of the above methods, a conservative shadow is extracted at two-dimensional stations corresponding to the location of an ice detector via a closest point method, and the results are transformed to plot shadow height as a function of angular position. By quantifying the shadow in this way and comparing it with the height of the ice detector, the functionality of the detector can be determined, allowing selection of optimal ice detector locations. Both methods of defining the shadow were validated with V-22 flight test data and, when used concurrently, provide the most conservative estimate for shadow height.

As the need for high fidelity methods has risen in all areas of CFD analysis, so has the need in droplet shadow prediction. Eulerian methods allow the droplet shadow to be

investigated across the entire aircraft without specifying areas of interest prior to analysis. The result is a comprehensive and unbiased solution for the placement of ice detectors according to the local shadow height. In addition, the use of CFD to determine the optimal placement of ice detectors can significantly reduce both the risks and costs associated with flight testing for ice protection systems.

REFERENCES

[1] Ruff, G.A., and Berkowitz, B.M., "Users' manual for the NASA Lewis ice accretion prediction code (LEWICE)". NASA Technical Report 185129, 1990.

[2] Bidwell, C.S., and Potapczuk, M.G., “Users manual for the NASA Lewis three-dimensional ice accretion code (LEWICE 3D)”, NASA Technical Report 105974, 1993.

[3] Beaugendre, H., Morency, F. and Habashi, W.G., “FENSAP-ICE’s Three-Dimensional In-Flight Ice Accretion Module: ICE3D,” Journal of Aircraft, Vol. 40, No. 2, 2003.

[4] Ballough, J., “Pilot’s Guide: Flight In Icing Conditions,” FAA, AC No. 91-74A, 31 Dec. 2007

[5] Abbott, I.H., and Von Doenhoff, A.E., *Theory of Wing Sections*, Dover, 1959.

[6] Flemming, R.J., Lednicer, D.A., "High Speed Ice Accretions on Rotorcraft Airfoils," NASA CR 3910, 1985.

[7] Bowden, D.T., Gensemer, A.E., and Skeen C.A., “Engineering Summary of Airframe Icing Technical Data,” FAA, Technical Report ADS-4, 1964.

[8] Messinger, B.L., “Equilibrium Temperature of an Unheated Icing Surface as a Function of Airspeed,” Journal of the Aeronautical Sciences, Vol. 20, No. 1, 1953, pp. 29-42.

[9] Morency, F., and Habashi, W.G., “Low-Water Concentration Zone Prediction with a 3D Eulerian Droplet Impingement Icing Code”, European Congress on Computational Methods in Applied Sciences and Engineering, Jyväskylä, Finland, 2004.

[10] Clift, R., Grace, J.R., and Weber, M.E., *Bubbles, Drops, and Particles*, Academic Press, New York, 1978, Chap. 5.

[11] Boutanios, Z., Bourgault, Y., Habashi, W.G., Isaac, G.A. and Cober, S.G., "3-D droplets impingement analysis around an aircraft's nose and cockpit using FENSAP-ICE". AIAA Paper 98-0200, January 1998.

[12] Bourgault, Y., Habashi, W.G., and Beaugendre, H., “Development of a Shallow Water Icing Model in Fensap-Ice,” AIAA 99-0246, 1999.

[13] Narramore, J.C., Tran, P., Baruzzi, G.S., Habashi, W.G., Akel, I., and Balage, S., “Ice Accretion Computations for Full Tiltrotor Configurations,” AHS 59th Annual Forum, May 2003.

[14] Al-Khalil, K., Salamon, L., and Tenison, G., "Development of the Cox Icing Research Facility," 36th Aerospace Sciences Meeting & Exhibit, AIAA 98-0097, January 12-15, Reno, NV, 1998.

[15] Lancaster, G.T., “Application of 3-D Computational Fluid Dynamic Icing Analysis to the V-22,” Bell Helicopter Textron Inc., Ft Worth, TX, 2008 (unpublished).

BIOGRAPHICAL INFORMATION

Glenn T. Lancaster graduated from Texas A & M University in 2004 with BS in aerospace engineering after which he began working toward a MS in aerospace engineering at the University of Texas at Arlington. He joined Bell Helicopter in 2005, while continuing graduate school, working in the aerodynamics group where he specializes in Computational Fluid Dynamic design and analysis. His work includes aircraft icing, air loads prediction, and high fidelity CFD analysis.